PREPRINT UCRL- 81545

Lawrence Livermore Laboratory

Survey of Mirror Machine Reactors

W. C. Condit

August 11, 1978

This paper was prepared for submission to the XVII Annual Enrico Fermi Summer School on Plasma Physics, September 4-16, 1978, Varenna, Italy.

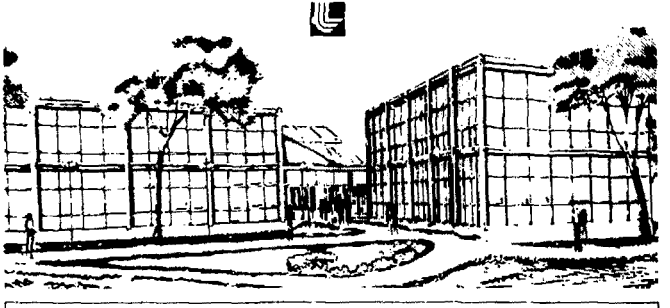

SURVEY OF MIRROR MACHINE REACTORS*

W. C. Condit
Lawrence Livermore Laboratory, Livermore, CA 94550

SUMMARY

The Magnetic Mirror Fusion Program is one of the two main-line fusion efforts in the United States. Starting from the simple axisymmetric mirror concept in the 1950's, the program has successfully overcome gross flute-type instabilities (using *minimum-B magnetic fields*), and the most serious of the micro-instabilities which plagued it (the drift-cyclotron loss-cone mode). Dense plasmas approaching the temperature range of interest for fusion have been created ($n_p = 10^{14}$/cc at 10-12 keV). At the same time, rather extensive conceptual design studies of possible mirror configurations have led to three principle designs of interest: The standard mirror fission-fusion hybrid, tandem mirror, and the field-reversed mirror. The lectures will discuss these three concepts in turn. There will be no discussion of diagnostics for the mirror machine in these lectures, but typical plasma parameters will be given for each type of machine, and the diagnostic requirements will be apparent. In a working fusion reactor, diagnostics will be required for operational control, and remarks will be made on this subject.

*Work performed under the auspices of the U.S. Department of Energy by the Lawrence Livermore Laboratory under contract number W-7405-ENG-48.

Lecture I: The Conventional Mirror Machine

W.C. Condit

One of the earliest phenomena in charged-particle physics to be thoroughly studied was the motion of charged particles in a converging magnetic field, and their tendency to "reflect" from regions of field significantly higher than the field at their point of origin. An example is shown in Fig. 1: This might be, for instance, a cosmic ray proton approaching the earth's magnetic pole. The original workers in this area (particularly Stormer) were motivated by astrophysical applications such as the trapping of charged particles by the earth's magnetic field.[1] Modern workers in the early 1950's proposed the reflection phenomenon as a way to confine plasmas for terrestrial experiments, principally aimed at the prediction of controlled thermonuclear reactions.[2] Details of this process were given in the lecture by Dr. Osher yesterday, but, for review, Fig. 2 shows typical particle orbits in a "simple magnetic mirror" formed by a pair of circular coils. The vacuum field is weakest in the mid-plane, and is weakened further as one enters the plasma by the diamagnetic effect of the plasma particles. If the particle velocity vector makes a large enough angle with the magnetic field as the particle crosses the mid-plane, it is confined. The criterion is, neglecting electrostatic effects

$$\frac{v_\perp^2}{v_\perp^2 + v_\parallel^2} = \sin^2\theta = \frac{B_0}{B_m} \qquad (1)$$

where B_0 is the mid-plane field and B_m is the mirror field. The ratio $R = B_m/B_0$ is the mirror ratio. The confined particles can be represented as an area on a $v_\perp - v_\parallel$ graph (Fig. 3).

As particles collide with each other in a mirror trap, they eventually scatter into the "loss-cone" of Fig. 3. The characteristic time for this to occur is τ_{ii} for ions and

$$\tau_e = \left(\tau_{ee}^{-1} + \tau_{ei}^{-1} \right)^{-1}$$

for electrons. Electrons scatter faster than ions, so electrons escape preferentially, leaving the plasma at a positive potential just sufficient to balance the electron and ion loss rates. This ambipolar potential enhances the ion loss rate somewhat above the ion scattering time, enlarging the "loss cone" to that region defined by the dashed line in Fig. 3. The net result is a particle loss rate proportional to the ion-ion scattering time, with a weak dependence on the mirror ratio:

$$n_t = 2.2 \times 10^{13} (E_i/100)^{3/2} \log_{10} R \qquad (2)$$

The constant of proportionality has been chosen to fit detailed kinetic-equation calculations of the collisional and ambipolar processes.[3] E is in kilovolts, and R is the net mirror ratio from mid-plane to mirror throat, averaged over the entire plasma, including the effects of the plasma in depressing the central field in its

interior. It will be noted that the $n\tau$ given by Eq. (2), even at 100 keV and reasonably high mirror ratios, is well below the commonly quoted "Lawson Criterion" of $n\tau \sim 10^{14}$, appropriate to net power production at optimum temperatures, with conventional steam-driven energy conversion systems. Thus the conventional mirror machine is forced to use very high temperatures and advanced energy recovery schemes to provide net energy output. The plasma must be maintained with high-efficiency neutral injectors, the escaping charged particle energy must be recovered at efficiencies considerably above 50%, and the neutron energy released by the fusion reactions must be run through a high-multiplication tritium-breeding blanket to get a useful device. Such a fusion reactor, using so-called "Yin-Yang" coils for plasma stability, is shown in Fig. 4a-b and its parameters are given in Table 1. The costs of this reactor are a sensitive function of the mirror ratio (because, although Eq. (2) has a weak dependence, the cost of the magnets goes up rapidly as larger fields are required to give larger values of R). See Fig. 5. The costs of mirror reactors also have an optimum when plotted against injection energy, because the fusion reactivity parameter begins to decline above 100 keV, and, while the confinement gets better, the power density (and gross power output of a given machine) drops to uninteresting levels for temperatures much above 300 keV (Fig. 6). This occurs because power density varies as $n^2\overline{\sigma v}(T_i)$, and the plasma density, n, is currently thought to be limited by the conditions[4]

$$\beta = 8\pi \sum_i n_i E_i \Big/ B_0^2 \leq \beta_* < 1 \qquad (3)$$

for "large" mirror machines - i.e. machines which are many gyroradii across. The upshot is that the conventional mirror machine is in principle capable of producing net power, but does not, under present knowledge, look like a good candidate for producing economical power. I keep repeating the phrase "under present knowledge," because there is some possibility that condition (3) can be relaxed, and this will be discussed in Part III of these lectures (Field Reversal).

An additional complication in any plasma with a loss-cone distribution of energies (Fig. 7a) is the presence of microinstabilities such as the "Drift-Cyclotron Loss-Cone" mode.[5] This mode is driven by the deviation of the distribution function from an isotropic Maxwellian distribution and will, if not checked, scatter medium energy particles into the ambipolar hole at a rapid rate, until the hole is filled and marginally stable (Fig. 7b). By partially filling the ambipolar hole (filling it at low energies), this instability can be stabilized, as shown in the 2XIIB experiments of 1974-1975. The technique involves injection of a warm plasma from the end of the machine along field lines. This causes the distribution to appear as in Fig. 7c. The average energy of ions in the hole is lower than in Fig. 7b, so the ion power drain is less. While not completely stable, the RF for distributions such as 7c can saturate at levels low enough so that it is not in itself a serious energy drain. The penalty one pays is an additional energy loss from the hot ions to the unconfined "stream" plasma. The effect is predicted to be less

serious for "large" machines, Figs. 8 and 9, but, even for the reactor parameters of Table I, one is on the verge of having trouble, since the quantity "R_p" in Figs. 8 and 9 is really the density gradient length $n_{max}/(dn/dr)$. As indicated in Fig. 8, the MFTF experiment will test these theoretical predictions.

I should add in closing that the conventional mirror does look attractive as a fission-fusion hybrid reactor.[6] Fig. 10 shows the power flow for a reactor, similar in design to that of Table I, but using an energy-multiplying fissionable blanket. The combination of net power out at lower fields, plus net fissile breeding, makes this approach attractive in a fission economy.

Lecture II: The Tandem Mirror

W. C. Condit

Early workers in the Magnetic Fusion Program realized that a long, straight solenoid with some type of "end plug" would make an attractive fusion reactor, and that one could pay for any extra energy input required in the plug region by lengthening the solenoid section.[7] We have seen in the previous lecture that the conventional magnetic mirror is not economically adequate as a magnetic "plug" by itself. However, if two high-density, marginal-gain mirror cells are placed at the ends of a low-density solenoid, the ambipolar potential of the end cells will confine the lower-energy solenoid ions.[8,9] This is the tandem mirror concept. A sketch of the physical situation is shown in Fig. 11, and the analysis in terms of the plug density, n_p, electron temperature, T_e, and central ion density and temperature, n_c, T_c, is given in Fig. 12. Plasma is supplied to the central solenoid at an ionization rate of j_c ions/(cc-sec) by cold gas or low energy neutral beams. The potential in the central cell is above "ground" but below that of the end cells. The ion confinement time can be approximated by the formula of Pastukhov,[10] showing a considerable lengthening of the containment time over τ_{ii}. The solenoid ion temperature and the electron temperature (which is constant throughout the machine) are given by straightforward energy - balance relations (Figs. 12,13). A sample set of reactor parameters is shown in Table III.[11,12] The plug injector energy is very high, because one wants to get the plug ions well above the ambipolar potential in the plugs, which in turn is considerably hotter than the (fusion temperature) plasma in the central cell. The plugs are run at the highest fields felt to be technologically sound for large magnets, in order to get the ratio of n_p/n_c as high as possible for n_c values which give economical power densities. The actual design in Table III is the result of a series of trade-offs (Figs. 14-16). A conceptual layout of the final reactor is shown in Fig. 17, and the power flow diagram is shown in Fig. 18.

Finally, one can run the tandem in a "two-component" mode, with high energy deuterons confined between the inner magnetic mirrors of the plugs, and lower temperature (5-6 keV) tritons confined electrostatically. Because the requirements of the electrostatic barrier are reduced considerably from those in Table I, the plug energies and densities can be reduced (Table IV). The resulting reactor, with $Q = 1.1$, is suitable for a fission-fusion hybrid.[12]

Lecture III: The Field-Reversed Mirror

W.C. Condit

As mentioned in the lecture on conventional mirror machines, the plasma pressure for a conventional mirror machine is limited by the so-called "Mirror Mode" to a value

$$\sum_j n_j E_j = \beta (B_0^2/8\pi) \leq \beta_c (B_0^2/8\pi) \qquad (4)$$

where $\beta_c \leq 1$. Experiments in 2XII-B, however, have achieved values of $\beta = 2$, if one bases the calculation on the ratio of the plasma pressure to the pressure of the external magnetic field.[13] This is possible because the field of the plasma diamagnetic currents adds to the confining field on the outside of the plasma. (pinch effect) In fact, the diamagnetic current can become so strong that the (BR,BZ) lines close within the plasma, eliminating the "loss cone," and changing the particle loss mechanism to a diffusive one,

$$\tau = (a^2/\rho_i^2)\,\tau_i \qquad (5)$$

where a is the plasma minor radius, ρ_i is the ion gyroradius, and τ_i is the 90^0 scattering time of the ions as they are scattered by all other species. For a moderately large value of (a/ρ_i) this time is much longer than given by Eq. (2). In addition, in classical theory,[14] the value of τ_i to be inserted in (5) is τ_{ei}, which is longer than τ_{ii} by roughly $\sqrt{m_i/m_e}$, giving an additional favorable factor. As we will see, however, (5) roughly describes the ion energy confinement time of the plasma if $\tau_i = \tau_{ii}$ -- i.e. in the classical case, ions must be supplied to the plasma at energies far above the mean, since the energy loss time is much faster than the particle loss time.

The idea of a closed field-line geometry using a purely poloidal field, with field lines encircling an azimuthal current, was proposed early in the CTR program for the toroidal Z-pinch[15] and the Astron thermonuclear reactor.[16] The idea is shown schematically in Fig. 19. In the Ion Astron reactor design,[17,18] the azimuthal current was carried predominantly by high energy beam protons - those with enough energy to encircle the axis of the device in roughly circular orbits. The D-T fuel ions were at a much lower average energy. In the course of the Astron work, it was noted that a significant fraction of the current could be contributed by the low energy, fuel ions, via the diamagnetic effect.[17,18] The Field-Reversed-Mirror lies at a limit of this process: a field-reversed configuration, localized by a weak mirror field, in which the azimuthal current is provided entirely by diamagnetic current. There is, of course a continuous transition from the Astron to the FRM case. Reactor designs in the Astron limit were studied extensively in the early 1970's.[18] They seemed very attractive, but of large unit size (about 5 to 6 gW_e). In this paper, we will study reactor parameter sets in the FRM limit, and will find that much smaller reactor units can be designed.

The quantitive distinction between an Astron geometry and an FRM geometry is best made on the number of gyroradii included in the minor radius of the plasma. If the characteristic gyroradius ρ_i is a small fraction of the minor radius a, one has the FRM. In this case the characteristic ρ_i is based on the mean ion energy. On the other hand, if the characteristic ion (or electron) gyroradius based on the injection energy satisfied ρ_i(or ρ_e) > a, one has the Astron case. In this latter limit, stable E-layers have recently been observed.[19] Experimental work by a group at the Kurchatov Institute[20] has also shown that field reversal at $(a/\rho_i) \approx 5$ in toroids with "greatly diffused" current sheaths is also apparently stable - the plasma survives for a hundred or more sound transit times across the major radius.

A theoretical framework for analyzing the stability of field-reversed layers has been developed.[21] It casts the stability criterion in the form of an energy principle with five terms, three of which are familiar from zero gyroradius stability theory. These three terms on balance indicate instability, and the effect of the new terms, which can be seen to have a stabilizing influence in certain limits, is under study. Examples of layers which are stable have not, as of this writing, been found. This is thought to be due to failure to search out the relevant parameter space for the "new" terms; it may, however, be due to omissions in the theory (which does not consider line-tying of the open field lines). Therefore, we rely on the above-mentioned experimental results.[20] Since the ratio $S = a/\rho_i$ was about 5 for stable plasmas in the Russian work (see Appendix C of Ref. 1 for a more detailed analysis), we have assumed S = 5 in our work. The Russian workers made no attempt to sustain their field-reversed configuration with neutral beam injection, but we will assume, for purposes of evaluation, that this can be done. We will further assume the FRM current layer can be established in situ at full magnetic field. One possible means for accomplishing this is a high-voltage pulsed ion diode of the type currently under development at several laboratories.[22]

Computation of Plasma Parameters

In order to evaluate the field-reversed mirror, it is necessary to compute the expected plasma parameters. To do so, we have formed a simple model with a number of free parameters which can be adjusted to fit experimental measurements or other, more detailed, theoretical calculations. We consider only conditions in the toroidal reversed field layer since the surrounding plasma is assumed to be confined only by weak mirrors; ions which diffuse into this region will be quickly lost. Basic to the model are equations for the central ion number density n_i and the mean ion and electron energies E_i and E_e. We assume an isothermal plasma and only one average ion of mass A_i = 2.5 AMU, and allow for the expected density gradient by an imposed density profile of cubic shape. We take particle and energy losses to be diffusive in nature and neglect the α-particles. Except for very high-energy beams, the α gyroradius (at 3.5 MeV) will exceed the plasma dimensions; they will

thus be lost essentially without energy deposition in the plasma. With these assumptions the appropriate zero-dimensional equations are

$$\frac{\partial n_i}{\partial t} = 0 = \dot{n}_0 - \frac{n_i}{\tau_p} \tag{6}$$

$$\frac{\partial n_e E_e}{\partial t} = 0 = Q_{ie} - \frac{n_e E_e}{\tau_{Ee}} - \frac{5}{3}\frac{n_e E_e}{\tau_p} - \dot{Q}_s - \dot{Q}_B \tag{7}$$

$$\frac{\partial n_i E_i}{\partial t} = n_0 E_{IN} - \frac{n_i E_i}{\tau_{Ei}} - \frac{5}{3}\frac{n_i E_i}{\tau_p} - Q_{ie} \tag{8}$$

$$n_e = n_i \tag{9}$$

$\dot{n}_0$ is the rate of increase of central density due to beam deposition, E_{IN} is the beam energy (assumed the same for D and T), and τ_p, τ_{Ee} and τ_{Ei} are, respectively, the particle, electron energy and ion energy confinement times. Q_{ie} is the ion-electron energy transfer rate per unit volume, for the assumed Maxwellian distribution function if ions and electrons given by[23]

$$Q_{ie} = \frac{n_i (E_i - E_e)}{\tau_E}, \quad (W/m^3), \tag{10}$$

$$\tau_E = \frac{5.396 \times 10^{18} A_i E_e^{3/2}}{n_e Z^2 \ln\Lambda} * \left[1 + \frac{\bar{E}_i}{1836 A_i E_e}\right]^{3/2} \tag{11}$$

with E in keV and n_e in m^{-3}. $\ln\Lambda$ has been taken as the typical value of 20 for these calculations. The cyclotron and bremsstrahlung loss terms are computed from standard expressions.[24,25] For the synchotron losses, the wall reflectivity has been taken as 0.8.

The magnetic field is related to the plasma pressure via the total β. We take β as given, either from experiment or from an equilibrium code, and compute B_0 along with the solution to the other equations from

$$B_0 = \left[\frac{2.68 \times 10^{-22}}{\beta}\left(n_e E_e + n_i E_i\right)\right]^{1/2} \quad \text{(Tesla)} \tag{12}$$

For the present calculations we have assumed $\beta = 1.5$, a value observed in 2XII8 (apparently without field reversal, however).[26]

For given confinement times, a very large family of solutions to Eqs. (1) - (10) depending on both n_0 and E_{IN} is possible. However, as discussed earlier, diffuse density profiles are expected, so we choose the characteristic beam attenuation length of the plasma to yield a cubic profile. The fraction of neutral beam which penetrates a distance x into the plasma is given by

$$f(x) = \left[\exp - \int_0^x \langle\sigma\rangle_T \, n_i dl\right] \tag{13}$$

where $\langle\sigma\rangle_T$ is the sum of the cross sections for ionization and charge-transfer[15] averaged over the ion and electron Maxwellian velocity distributions. For radial beam injection, the distance x is measured along the plasma radius. For isothermal plasmas with density profiles of the form $n = n_0(1 - r^j/a^j)$ where r is the radial distance from the minor axis, Eq. (13) becomes

$$f(x) = \exp\left[- \frac{j}{j+1} \, n_i \, \langle\sigma\rangle_T \, x\right]. \tag{14}$$

Results for the mirror FERF design[28] suggest that a cubic profile (j=3) can be expected for radial injection if $f(2a) = \exp(-1.75)$. It is clear that we can obtain this value by adjusting n_0 to yield the desired f(2a) through its dependence on n_i. Note that $\langle\sigma_T\rangle$ depends also on E_i, E_{IN} and E_e, albeit only very weakly on the latter.

To complete the description, we need expressions for the particle and energy confinement times. The classical result of $\tau_p, \tau_{Ee} = a^2\tau_{ei}/\rho_e^2$ where ρ_e is the electron gyroradius and τ_{ei} is the electron-ion scattering time has seldom been observed in experiments. We have therefore made the more conservative assumption of

$$\tau_p = a^2\tau_{ii} \, f(j)/\rho_i^2$$

$$\tau_{Ee} = \tau_{Ei} = a^2\tau_{ii}/\rho_i^2 \tag{15}$$

where ρ_i is the ion gyroradius and τ_{ii} is given by[29]

$$\tau_{ii} = 3.58 \times 10^{14} \, \frac{A_i^{1/2} \, E_i^{3/2}}{n_i \ln\Lambda} \tag{16}$$

f(j) is a factor which accounts for the effect of the cubic density profile. In Eq. (11) the mean number density $n_i (= \bar{n}_i)$ for the plasma is used.

We have also considered Bohm diffusion as a loss mechanism. This amounts to estimating the diffusion coefficient as $D = \rho_{ce}^2\omega_{ce}/8$.[30] At the high temperatures and modest magnetic fields and densities we are considering for the FRM reactor, Bohm diffusion is 8 to 12 orders of magnitude faster than classical diffusion and, since $\rho_e^2 = \rho_i^2(m_e/m_i)$, it is well over 5 orders faster than the ion loss rates we used in the energy balance calculations. It is clear that any

loss rate approaching the Bohm rate will be fatal to the FRM. Also, since the size of the plasma appears to be limited to a small number of gyroradii, one cannot avoid the problem by going to a large plasma minor diameter.

The above equations have been combined in a computer code which enables all quantities to be evaluated as a function of the neutral-beam energy E_{IN}. Calculations have been made for a torus of circular cross section and one with a highly elongated cross section. The latter yields higher values of Q and appears possible from both experiments[19] and theory. Similarly, a torus with aspect ratio near unity is indicated; we have taken the major radius R = 2a. Results for this case are plotted in Fig. 20 for $S = a/\rho_i = 5$ and a length/radius ratio l/a = 3. We note quite favorable Q values (for D-T and a fusion energy of 17.6 MeV) of 4-6 for beam energies of 150-300 keV. At the higher beam energies, the required magnetic field is quite high, but it appears that for a small penalty in Q we can lower the beam energy and thus the required B_0 to values attainable with inexpensive superconductors. The best combination of parameters is dictated by economic considerations which is the subject of the next section.

Reactor Parametes and Cost Estimates

In this section we first describe the overall configuration of an FRM power reactor. Then we will describe the details of our parametric analysis and cost estimates which we are using to optimize the design for minimum power cost. The parametric analysis and cost estimate are still in an early stage of development; so the resluts reported here should be considered preliminary.

We assume that an FRM Reactor would consist of a number of plasma layers (~ 10) on a common axis (see Fig. 21), held apart by weak magnetic mirrors are produced by water-cooled copper coils placed between the plasma and blanket. Also, copper Ioffe-bar conductors are placed at this location to form a magnetic well.

The neutron moderating blanket and the shield for the superconducting coil are cylindrical shells. We are considering both a high and low energy multiplication blanket. The high multiplication blanket contains beryllium and achieves an average M (blanket thermal energy per fusion neutron/14.1 MeV) of 1.7 through n, 2n reactions. The low multiplication blanket achieves an M of 1.2 due to exothermic neutron capture. Tritium is bred in solid lithium-containing compounds. The blanket is cooled by helium. Hot and cold mamifolds pass axially through the reactor, and individual axial segments of the blanket are cooled by parallel flow circuits. The exit helium is used to generate steam for a steam power cycle which has an efficiency of 40%.

As we will show, the optimum magnetic field strength for the superconducting solenoid appears to be about 10 Tesla, thus permitting the use of niobium-titanium superconductor. The superconducting solenoid is restrained by a simple hoop structure. Outside the coil and coil structure is a cylindrical vacuum vessel.

Neutral beam injectors are arranged along the length of the reactor, aimed radially inward. As we will show, injection energies of ≥ 200 keV are desirable thus necessitating the use of negative ion type neutral beam injectors for high injection efficiency (≥ 80%).

At each end of the reactor, a single-stage direct converter converts about 50% of the energy of the plasma end leakage directly into electricity. The remaining energy is removed by helium coolant and added to the steam power cycle. The direct converter chambers contain the primary vacuum pumping system for the reactor, consisting of 4^{0} K helium-cooled condensation panels.

The entire reactor, including the injectors and direct converters, is assumed to be oriented vertically and enclosed in a reinforced concrete containment building. Depending on the desired electrical output of the power plant, more than one reactor may be placed in the same building.

Now we will describe the step-by-step procedure used in the parametric analysis to design a particular reactor. The primary independent physics parameter has been taken to be the injection energy. The physics model of Section III then yields the required magnetic field strength, the size of the plasma layer, the plasma energy and density, the fusion power and the plasma Q (fusion power divided by injected neutral beam power). Some of these results are shown in Fig. 20. The fusion power is shown in Fig. 22. For each value of injection energy the engineering design begins with the coupled problem of the internal dimensions (radius and length) of the reactor cell and the design of the copper coils. First we specify a trial length L for the reactor cell. Then, adding the neutron flux contribution from each plasma layer, the first wall radius R_w is set so that the peak first wall neutron wall loading, Γ_N is a preselected value. For the cases discussed in this paper we have set $\Gamma_N = 4\ MW/m^2$, based on typical results from the Yin Yang mirror reactor study.[31] For simplicity, we assume that the mirror coils, Ioffe bars, and blanket first wall are all at the first wall radius. This is a good approximation since the copper coils are always small in cross-section. There is a lower limit placed on the first wall radius: it is not allowed to be less than the radial extent of the plasma toroid plus two alpha particle gyroradii. At this point in the calculation we check to verify that the cell length L satisfies the criterion $L \geq 1.2\ R_w$. Below this spacing the axial mirror ratio (coil to center) of a pair of coils is less than unity. The optimum distance from an economic point of view always turns out to be somewhat greater than this minimum spacing, because as this spacing is approached, very large mirror currents are required to maintain the mirror ratio greater than unity. (See Figure 23) With the mirror coils defined in length and radius, the axial mirror ratio may be varied by changing the mirror coil current. (Recall that a large uniform solenoidal field is established by the superconducting coil.)

Just how much axial mirror ratio is necessary is not obvious. Indeed, it is conceivable that the plasma layers could be stable in a uniform field. However, for this study, we have required a small axial mirror ratio of 1.0001; this ratio is

defined to include the fields from all coils and all plasma layers except the one in the cell under consideration i.e. it is the "vacuum" mirror ratio seen by the plasma layer. For the current in the Ioffe bars we require a small radial well of 1.0001 at the plasma major radius. An approximate formula of Taylor[32] is used for this calculation; more accurate coil calculations may show the well to be somewhat different. Although the above choices of mirror ratios are somewhat arbitrary, the resultant mirror coils and Ioffe bars contribute a negligible amount to the overall reactor cost and higher currents could be specified.

Now we must determine the cross-sectional area of the copper mirror coil and Ioffe bars. An economic trade-off exists: large cross-section coils will minimize the resistive power loss in the coils, but maximize the neutron attenuation in the coils. We perform an optimization to minimize the sum of the resistive loss in the coils and the potential for electrical power production which is "lost" because of neutron attenuation in the copper. The latter quantity is approximated by multiplying the neutron heating of the copper by M and by the thermal efficiency of the steam power cycle. Within this optimization is another optimization such that, for a given total resistive loss in the coils, the loss is apportioned between the mirror coils and Ioffe bars so that to minimize neutron interception. This completes the design of the reactor cell and copper coils for a single trial cell length.

In general, larger trial cell lengths result in smaller first wall radii (because of the criterion on neutron wall loading) and smaller copper coil losses. The calculation of all costs determines the optimum cell length for the injection energy being considered. Because the first wall radius is a weak function of cell length and the copper coil losses tend to be quite small, we have found to date that small cell lengths rather close to the minimum allowed are best.

The remainder of the reactor is designed from the first wall outward. The thickness of the cylindrical shell blanket is set at 1 meter. The design thickness for the superconducting coil shield involves an economic trade-off. Thicker shields reduce the neutron heating of the coil and thus the cost of cryogenic refrigeration, but they increase the size and cost of the coil, coil structure, vacuum vessel, and the containment building. We calculate an optimum shield thickness for each case. However, because of the exponential attenuation of neutrons in the shield, we have found that the optimum shield thickness is always in the narrow range of 70 to 80 cm. The superconducting solenoid is placed outside the shield. The thickness of the coil restraining structure (a single stainless steel cylindrical shell) is calculated based on a 60,000 psi design stress. The main vacuum tank surrounding the coil structure was assumed to be aluminum, and was designed to ASME code as a long cylindrical vessel. (This neglects the stiffening effect of the ends and any webbing, and thus overestimates the weight.) The containment building is sized to hold the reactor, complete with its injectors and direct converters. We have not yet designed the components of the reactor in much detail, but they are in most cases simple (circular coils, cylindrical tanks, etc.) and we feel that adequate prelim-

inary cost estimates can be made. We have calculated direct capital costs using 1975-76 prices except where noted, and have not included indirect cost factors for construction facilities, engineering, interest during construction, contingency, etc. Table V gives the basis for our preliminary cost estimates. For a number of components, the estimates were borrowed from other reactor studies conducted at LLL, and are not based directly on the concurrently developed FRM design shown in Fig. 21. In future work we will be able to improve our cost estimates for these components. Although all of the estimates are subject to change and additional cost categories may be added, we believe our present results to be reasonably accurate.

The $/kWe cost of the reactor is calculated by dividing the total direct captial cost by the net electric power of the plant. Figure 22 shows this cost as a function of injection energy for cases of optimum cell length. Curves are shown for two values of blanket energy multiplication, M = 1.2 and 1.7. We see that the minimum costs occur for injection energies near 250 keV. The minimum cost is $950/kWe for M = 1.2 and $730/kWe for M = 1.7. Also shown on Figure 22 are the fusion power and the net electric power per reactor cell.

Figure 22 shows that the cost variation is quite small over a range of injection energy from 200 to 300 keV. At lower energies the cost increases primarily because of lower Q's and the resulting high recirculating power fractions. At higher energies the cost increases because the more slowly increasing Q no longer compensates for the higher magnetic field strengths which are required. For the M = 1.7 blanket, the magnet and magnet structure accounts for 16 % of the total cost at the optimum injection energy, but for 400 keV injection these costs are 38% of the total.

Table VI gives reactor parameters for a near-optimum design with M = 1.7. We chose the slightly off-optimum case with 200 keV injection energy because the required superconductor field strength is lower, making possible the use of niobium-titanium superconductor. The optimum design occurs for 250 keV injection. The power output (23 MW/cell) and B field (110 kilo Gauss) are slightly higher than the case in Table V, and the plasma dimensions are slightly smaller. The power cost for this high field case is only about 2% lower than the cost in Table V.

The reactor costs shown in Fig. 22 are extremely attractive. This was perhaps to be expected a priori for a system with high β and simple magnetic field configuration. We are making a detailed engineering design of a reactor with the parameters given in Table VI, and are concurrently working to reduce the number of physics extrapolations and assumptions needed. We feel confident that, if questions such as the start-up and maintenance of an FRM configuration can be answered with reasonable technology, the end product will be a very useful form of CTR reactor.

References

1. STORMER, C., Arch. Sci. Phys., Geneve, 24 (1907) 5, 113, 221, 317.
2. POST, R.F., "Experimental Research on High-Temperature Plasmas," Proc. Second U.N. Int. Conf. on Atomic Energy, U.N., N.Y. 32 (1958) 245.
3. MOIR, R.W., Ed., "Standard Mirror Fusion Reactor," Lawrence Livermore Laboratory, Livermore, CA, UCID-17644, Table 5-1 (Table 1 of present paper).
4. Ibid., page 5-6.
5. BALDWIN, D.E., "End Loss Processes from Mirror Machines," Lawrence Livermore Laboratory, Livermore, CA, UCRL-78406, (1976).
6. BENDER, D.J., Ed., "Reference Design for the Standard Mirror Hybrid Reactor," Lawrence Livermore Laboratory, Livermore, CA, UCRL-52478, (1978).
7. YORK, H., quoted by R.F. Post, in "Lectures on Controlled Thermonuclear Reactions," Lawrence Livermore Laboratory, Livermore, CA, UCRL-4231, 1954.
8. DIMOV, G.I., et al., "Open Trap with Ambipolar Mirrors," Proc. Sixth Inter. Conf. on Controlled Nuclear Fusion, Berchtesgaden, Fed. Rep. of Germany, 1976 (IAEA).
9. FOWLER, T.K., LOGAN, B.G., "The Tandem Mirror Reactor," Comments on Plasma Phys., 2, 167 (1974).
10. PASTUKHOV, V.P. "Collisional Losses of Electrons from an Adiabatic Trap with Positive Potential," Nucl. Fusion 14, 3 (1974).
11. MOIR, R.W., et al., "Preliminary Design of the Tandem Mirror Reactor," Lawrence Livermore Laboratory, Livermore, CA, UCRL-52302 (1977).
12. LOGAN, B.G., et al., "Tandem Mirror Reactors," Lawrence Livermore Laboratory, Livermore, CA, UCRL-80644 (1978). (To be published in Proc. Seventh Intern. Conf. on Plasma Phys., Innsbruck, Austria, 1978, IAEA)
13. COENSGEN, F.H., et al., Phys. Rev. Lett. 35, 1501 (1975), 37, 1468 (1976).
14. SPITZER, L., JR., "Physics of Fully Ionized Gasses," Interscience, NY., 1962.
15 TUCK, J.L., Proc. Second U.N. International Conference on Peaceful Uses of Atomic Energy, U.N., General 1958, Vol. 32, p. 3.
16. CHRISTOFILOS, N.C., Ibid, p. 279.
17. ANDERSON, D.V. et al., Proc. Fourth International Conference on Plasma Physics, Madison, 1971, Vol. I, p. 137 (IAEA, Vienna 1971).
18. CHRISTOFILOS, N.C., et. al., "Energy 70" Inter-society Energy Conference, p. 1-36.
19. BZURA, J.J., et al., Phys. Rev. Lett. 29, 256 (1972).
20. ESKOV, A.G., et al., Proc. 7th European Conference on Controlled Fusion and Plasma Physics, CRPP, Lausanne, 1975, p. 55 (see also Ref. 1, p. 20).
21. SUDAN, R.N. and ROSENBLUTH, M.N., Phys. Rev. Lett. 36, 972 (1976).
22. PRONO, D.S., et al., Proc. International Topical Conference on Electron Beam Research, (1975), Vol. I, p. 575; DI CAPUA M., et al., Ibid., p. 555; MILLER, P.A., et al., Ibid., p. 629.

23. MORSE, T.F., Phys. Fluids 6, 1420 (1963).
24. ROSE, D. and CLARK, M., "Plasmas and Controlled Fusion" (J. Wiley, N.Y., 1961).
25. TRUBNIKOV, B.A., JETP Letts. 16, 25 (1972).
26. COENSGEN, F.H., et al., Proceedings Sixth International Conference on Plasma Physics and Controlled Nuclear Fusion, (1976).
27. RIVIERE, A.C., Nucl. Fusion 11, 363 (1971).
28. BATZER, T.H., et al., Lawrence Livermore Laboratory, Livermore, CA, UCRL-51617 (1974).
29. BRAGINSKII, S.I., in Reviews of Plasma Physics, Ed. by M.A. Leontovich (Consultants Bureau, NY., 1965).
30. SPITZER, L., Phys. Fluids 3, 659 (1960).
31. CARLSON, G.A., MOIR, R.W., "Mirror Machine Reactors,"
32. TAYLOR, J.B., in Plasma Physics, (IAEA, Vienna, 1965), p. 449.
33. POWELL, J.R., Proc. Conf. Applied Superconductivity, 1972, IEEE 72 CHO-5-TABSC, P. 346.
34. MOIR, R.W., et al., Lawrence Livermore Laboratory report on mirror reactor study to be published.
35. BATZER, T.H. et al., "Conceptual Design of a Mirror Reactor for a Fusion Engineering Research Facility (FERF)", Lawrence Livermore Laboratory, Livermore, CA, UCRL-51617, Aug. 1974.

Figure Captions

Fig. 1 Orbit in a converging field.

Fig. 2 Orbit of particles in a mirror field (note field depression near axis due to plasma).

Fig. 3 "Loss-cone" boundaries without (———) and with (-----) ambipolar potential.

Fig. 4a. Plasma and coil geometry for mirror reactor.

Fig. 4b Schematic of standard mirror reactor.

Fig. 5 Variation of power cost and wall neutron flux with vacuum mirror ratio. (From Ref. 3)

Fig. 6 Variation of power cost and wall neutron flux with injection energy. (From Ref. 3)

Fig. 7a Classical ion distribution for total R = 6. No warm component.

Fig. 7b Schematic ion distribution for marginally stable state with no stream. Note characteristic peak at beam E_b.

Fig. 7c Ion distribution with warm component partially filling ambipolar hole. Peak is slightly below E_b in the experimental observations. The width of the warm component is exaggerated for clarity: It may actually be much narrower than .1 E_b.

Fig. 8 Stability boundaries for the drift cyclotron loss-cone instability. Also plotted is the expected electron temperature, T_e, for MX (now called MFTF) parameters and different amounts of streaming plasma, η_{warm}.

Fig. 9 Plasma "radius" for stability to the drift-cyclotron loss-cone (DCLC) mode as a function of $(\omega_{ci}/\omega_{pi})$ for various fractions of warm plasma.

Fig. 10 Reactor power flow for fission-fusion hybrid.

Fig. 11 Tandem mirrors with ambipolar barriers.

Fig. 12 Ion confinement in the solenoid is enhanced by potential barrier.

Fig. 13 Electrons are confined by net positive potential.

Fig. 14 Effect on cost of 1000-MW(e) TMR's of variation in (a) injection energy E_{inj}, (b) vacuum mirror ratio between the center of the plug and the central cell B_p/B_c, and (c) temperature of the ions in the central cell T_c.

Fig. 15 Effect on (a) predicted reactor cost and (b) recirculating power fraction f_r and neutron loading of the first wall Γ_n of variation in $B_{0,plug}$, the vacuum magnetic field strength at the center of the plug, for 1000-MW(e) TMR's with vacuum mirror ratio of the plug $R_{vac,\ plug}$ = 1.07.

Fig. 16 Predicted cost of optimized 1000-MW(e) TMR's as a function of the vacuum mirror ratio of the plug $R_{vac,\ plug}$ for plug mirror field B_{mirror} = 17.7 T.

Fig. 17 Tandem Mirror Reactor.

Fig. 18 TMR power flow diagram.

Fig. 19 Schematic of Field-Reversed Mirror Reactor.

Fig. 20 Mean ion and electron energies (E_i, E_e) magnetic field (B_0) and Q vs. neutral-beam energy for $a/\rho_i = 5$, $R_p/a = 2$, $L/R_p = 3$.

Fig. 21 Layout of Multi-cell FRM Reactor.

Fig. 22 Power cost and fusion power vs. injection energy for optimum cell lengths.

Fig. 23 Projected cost of electrical power vs. cell length.

Table I. Physics Parameters, Reference Case.

Distance between mirrors, L	16 m
Plasma radius, r_p	3.0 m
D^+ gyroradius a_i at B_0 and E_{INJ}	4.3 m
Mirror field, B_m	12.0 T
Vacuum central field, B_{vac}	4.0 T
Vacuum mirror ratio, R_{vac}	3.00
Net mirror ratio, R	6.54
Plasma pressure/vacuum field pressure, β	0.79
Density X containment time, $n\tau$	5.0×10^{13} s/cm^3
Fusion power/injected power, Q	1.2
Central electron density, n_0	1.58×10^{14} cm^{-3}
Reaction rate parameter, σv_{DT}	7.57×10^{-16} cm^3/s
Fusion Power, P_F	1266 MW
Power injected and trapped, P_{in}	1130 MW
Injected D^0 current, I_{D^0}	4794 A
Injected T^0 current, I_{T^0}	2739 A
Injection energy, E_{INJ}	150 keV
Equivalent mid-plane injection angle, θ_{INJ}	65°
Mean kinetic energy of confined electrons (at mid-plane)	26 keV
Mean kinetic energy of confined deuterons (at mid-plane)	184 keV
Mean kinetic energy of confined tritons (at mid-plane)	209 keV
Mean kinetic energy of confined alpha particles (at mid-plane)	1330 keV
Electrostatic potential energy (mid-plane to mirror)	75 keV
Mean kinetic energy of escaping electrons (at the mirror)[a]	34 keV
Mean kinetic energy of escaping deuterons (at the mirror)	155 keV
Mean kinetic energy of escaping tritons (at the mirror)	160 keV
Mean kinetic energy of escaping alpha particles (at the mirror)[a]	358 keV
Electrostatic potential energy (mid-plane to direct converter)	94 keV
Mean energy of escaping electrons (at direct converter)	15 keV
Mean energy of escaping deuterons (at direct converter)	174 keV
Mean energy of escaping tritons (at direct converter)	179 keV
Mean energy of escaping alpha particles (at direct converter)[a]	395 keV

[a]Approximately 9 % of the alpha particles are born with velocities in the loss cone and are immediately lost.

Table II. Summary of reactor characteristics.

Magnet	
Central field, T	2.52
Mirror ratio	2.25
Max field at conductor, T	8.5
Injectors	
Type	Positive-ion acceleration
Extraction voltage, kV	
Deuterium	125.0
Tritium	187.5
Efficiency	0.58
Injected current, A	
Deuterium	3467
Tritium	1733
Plasma	
Av injection energy, keV	121
Plasma mirror ratio	4.15
Beta	0.71
Central plasma density, cm^{-3}	9×10^{13}
$n\tau$, s/cm^3	2×10^{13}
Q	0.64
Dimensions	
Mirror-to-mirror length, m	13.0
Radius at midplane, m	2.5
Blanket	
Fractional blanket coverage	0.86
Av blanket multiplication (86% coverage)	10.4
First-wall load, MW/m^2	1.7
Peak fuel power density, W/cm^3	280
Coolant	
Pressure, atm	60
Inlet/outlet temperatures, °C	280/540
End-of-life exposure, $MW\text{-}y/m^2$	6.6
Av fissile breeding ratio (86% coverage)	1.5

Table III. TMR Physics Parameters.

Parameter	Value
End Plug:	
Injection energy	1200 keV
Mean ion energy	880 keV
Plasma density	8.6×10^{14} cm^{-3}
Trapped current into each plug	220 A
Electron temperature	42 keV
$\beta_{plug}\left(\equiv \frac{p}{B_{vac}/2\mu_0}\right)$	1
Plasma radius	0.5 m
B_{vac} plug (midplane)	16.5 T
R_{vac}	1.07
Potential at midplane	350 keV
Particle $n\tau$	2.5×10^{14} s·cm^{-3}
Central Cell:	
Current injected	1570 A
β	0.7
Length	100 m
Plasma radius	1.2 m
B_{vac} (midplane)	2.4 T
Electron temperature	42 keV
Ion temperature	30 keV
Plasma density	1.1×10^{14} cm^{-3}
Particle $n\tau$	7.7×10^{14} s·cm^{-3}
Potential of plasma	260 keV

Table IV. Example Parameter Values for a Q = 1.1 Two-Component Tandem Hybrid Reactor

Parameter	Value
Solenoid Length, L_c	50 m
Solenoid radius, r_c	0.37 m
Solenoid electron density, n_c	1.7×10^{20} m^{-3}
Solenoid deuterium density, n_D	6.3×10^{19} m^{-3}
Solenoid tritium density, n_T	1.1×10^{20} m^{-3}
Electron temperature, T_e	6.0 keV
Injection energies, E_{inj}	200 keV
Solenoid field, B_c	1.8 T ($\epsilon_c = 0.8$)
Plug field, B_{0p}	7.0 T ($R_p = 2$, $\epsilon_p = 0.7$)
Plug density, n_p	4.6×10^{20} m^{-3}
Plug radius, r_p	0.16 m ($r_p/\rho_i = 12$)
Fusion power	410 MW
Neutron wall loading, (at 1-m wall radius)	1 MW/m^2

Table V: Basis for Cost Estimate

1)	Superconductor:	Present prices reduced by Powell 3.5 factor for mass production.[33]
2)	Winding	1/2 of Yin-Yang winding cost per A-m
3)	Structure	Stainless steel at $11/kg.
4)	Power supply	Porportional to coil energy, normalized to Ref. 35.
5)	Refrigeration system	Proportional to coil neutron heating, normalized to Ref. 34.
6)	Blanket (with beryllium)	$280 K/m^3.[34]
7)	Blanket heat transfer loop	$37/kW handled.[34]
8)	Shield	80% stainless steel at $11/kg.
9)	Vacuum tank	Aluminum at $22/kg.
10)	Vacuum pumping system	1/2 of vacuum tank cost.
11)	Neutral beam injectors	$200/kW injected.
12)	Diagnostics and control	$100 K/cell.
13)	Tritium handling systems	Normalized to Ref. 34
14)	Direct converters	$100/kW of charged particles.[34]
15)	Direct converter heat transfer loop	$35/kW handled.[34]
16)	Main containment building	Proportional to volume, normalized to Ref. 34.
17)	Thermal Conversion system	$20/kW handled.[34]
18)	Turbine building	$5/kW handled.[34]

Table VI. Typical FRM Reactor Design

Beam Energy - 200 keV

Plasma minor radius a = 0.031 m	Wall Radius 0.61 m
Plasma major radius R_p = 0.062 m	Cell length = 1.1 m
Plasma length = 0.19 m	Injected current = 17 A/cell
a/r_i = 5	Injected power = 3.5 MW/cell
Vacuum Field = 8.2 Tesla	
Ion Energy = 77 keV	Mirror coil current = 46 KA
Electron energy = 29 keV	Ioffe bar current = 10 KA
Peak Density = 3.6 X 10^{21} ions/m^3	Mirror coil cross section = 13 cm^2
Fusion Q = 5.3	Ioffe bar cross section = 14 cm^2
Fusion Power = 18.5 MW/cell	resistive power = 0.28 MW/cell
Plasma = 1.5	neutron heating = 0.38 MW/cell
Blanket thickness = 1 m	P_{net} = 10.2 MWe/cell
Blanket M = 1.7	Total cost = $745/kWe
Shield thickness = 0.8 m	
Superconducting solenoid radius = 2.4 m	

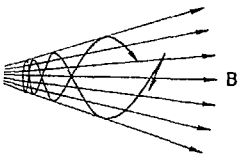

Figure 1: Orbit in a converging field.

ORBITS OF PARTICLES IN A MIRROR FIELD
(NOTE FIELD DEPRESSION NEAR AXIS DUE TO PLASMA)

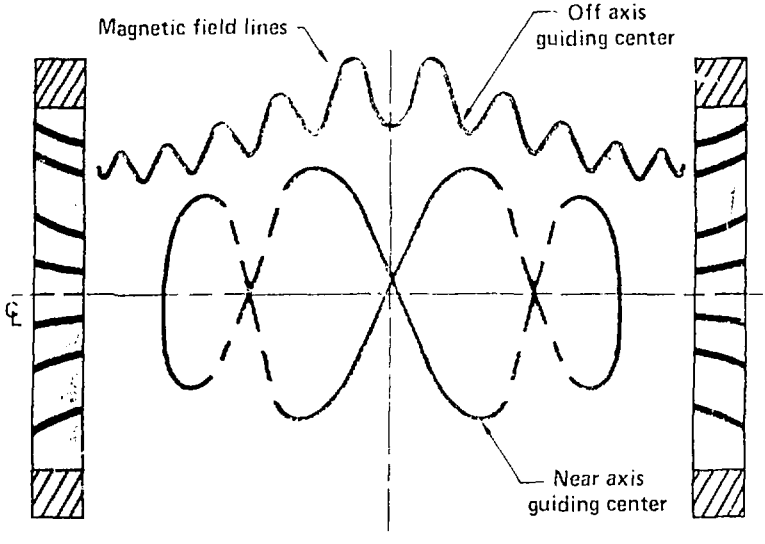

Figure 2: Orbit of particles in a mirror field (note field depression near axis due to plasma).

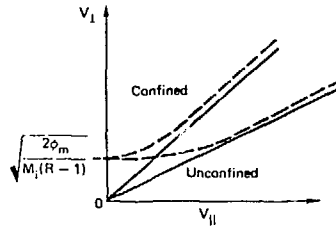

Figure 3: "Loss cone" boundaries without (——) and with (----) ambipolar potential.

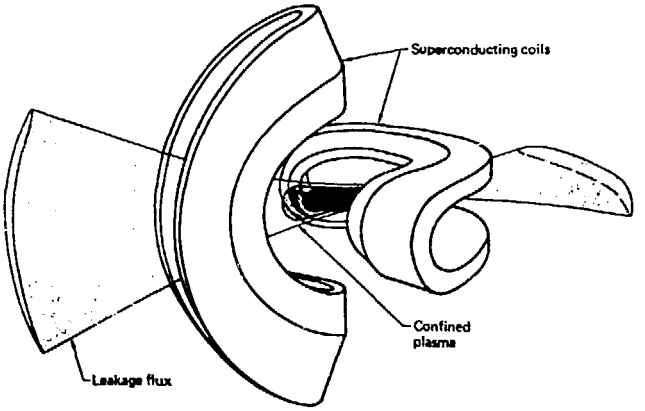

Figure 4a: Plasma and coil geometry for mirror reactor.

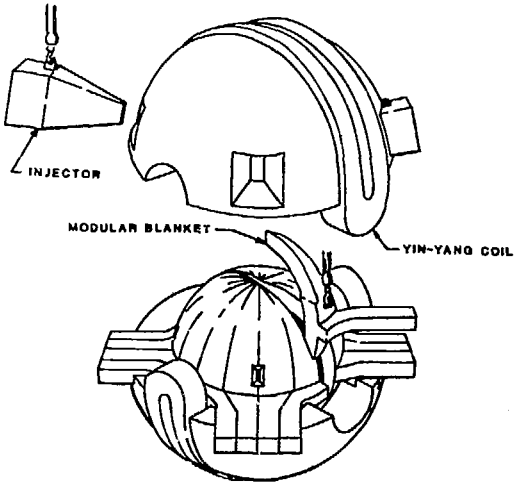

Figure 4b: Schematic of standard mirror reactor.

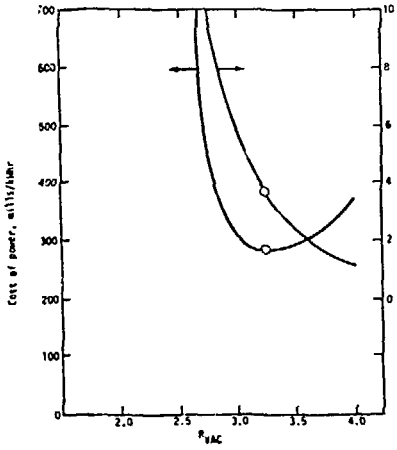

Figure 5: Variation of power cost and wall neutron flux with vacuum mirror ratio. (From Ref. 3)

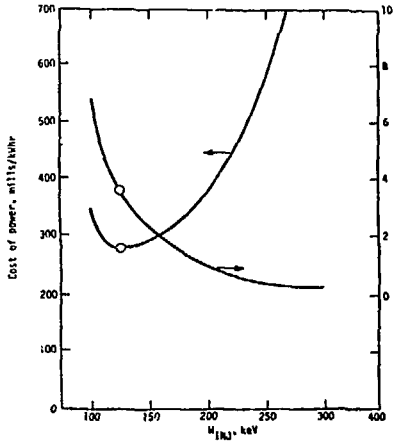

Figure 6: Variation of power cost and wall neutron flux with injection energy. (From Ref. 3)

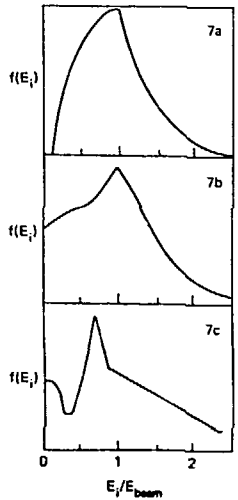

Figure 7a: Classical ion distribution for total R=6. No warm component.

Figure 7b: Schematic ion distribution for marginally stable state with no stream. Note characteristic peak at beam E_b.

Figure 7c: Ion distribution with warm component partially filling ambipolar hole. Peak is slightly below E_b in the experimental observations. The width of the warm component is exaggerated for clarity: It may actually be much narrower than .1 E_b.

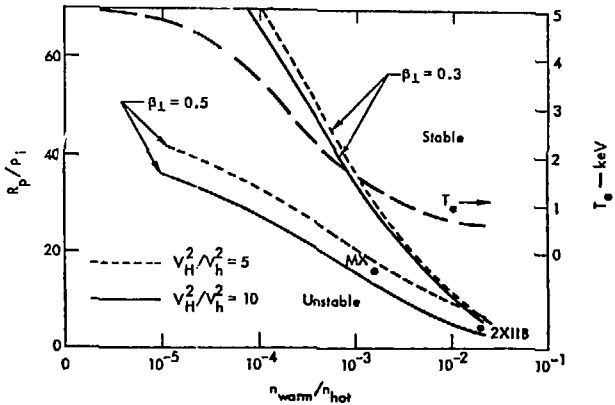

Figure 8: Stability boundaries for the drift cyclotron loss-cone instability. Also plotted is the expected electron temperature, T_e, for MX (now called MFTF) parameters and different amounts of streaming plasma, n_{warm}.

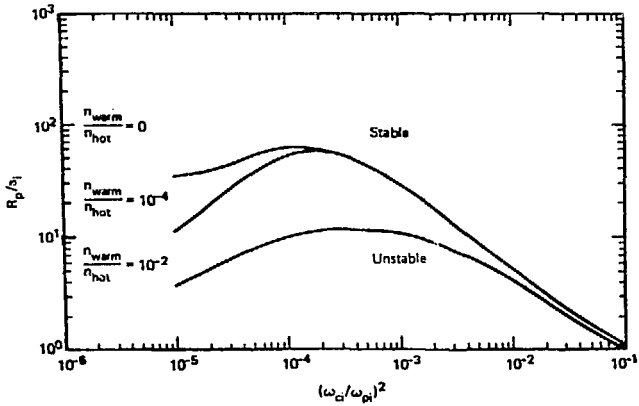

Figure 9: Plasma "radius" for stability to the drift-cyclotron loss-cone (DCLC) mode as a function of $(\omega_{ci}/\omega_{pi})^2$ for various fractions of warm plasma.

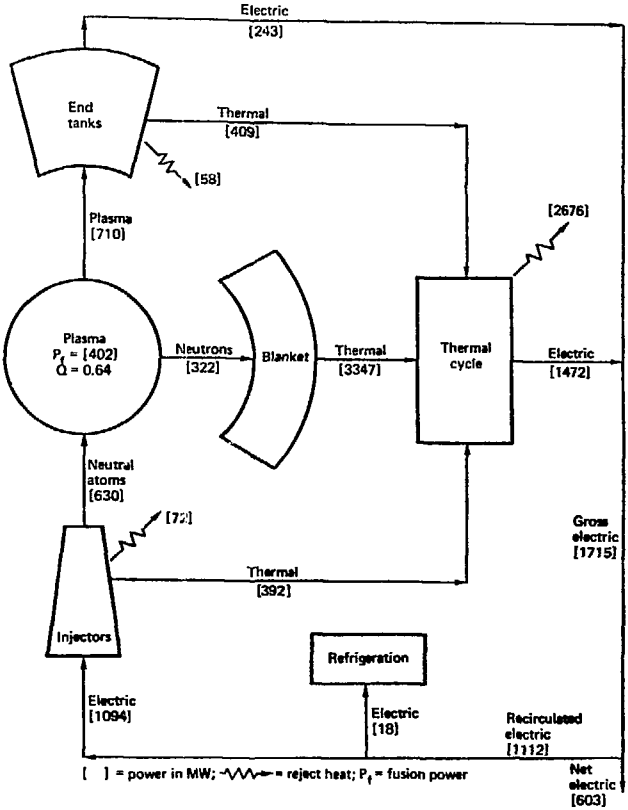

Figure 10: Reactor power flow for fission-fusion hybrid.

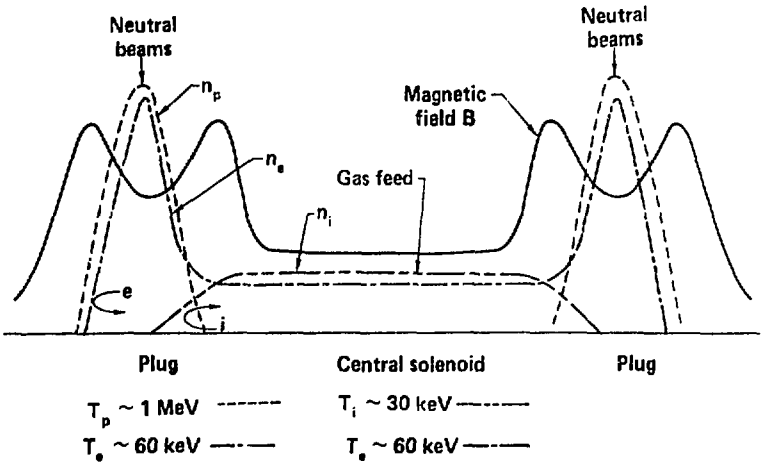
Neutral beams
Neutral beams
n_p
Magnetic field B
n_e
Gas feed
n_i
e
i
Plug
Central solenoid
Plug
$T_p \sim 1$ MeV
$T_i \sim 30$ keV
$T_e \sim 60$ keV
$T_e \sim 60$ keV

Figure 11

ION CONFINEMENT IN THE SOLENOID IS ENHANCED BY POTENTIAL BARRIER

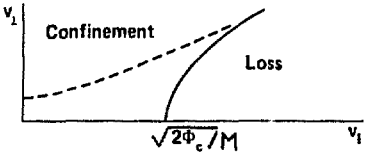

- Confinement

$$(n\tau)_c = n\tau_{ii}\, g\,(R) \left(\frac{\Phi_c}{T_c}\right) \exp \frac{\Phi_c}{T_c}$$

$$\phi(z) - \phi(0) = T_e \ln [n(z)/n(0)]$$

$$(n\tau)_c = n\tau_{ii}\, g\,(R) \left(\frac{T_e}{T_c} \ln \frac{n_p}{n_c}\right) \left(\frac{n_p}{n_c}\right)^{\frac{T_e}{T_c}}$$

Enhancement requires $n_p > n_c$

- Density

$$n_c^2 = (n\tau)_a\, j_c$$

- Temperature

$$\frac{3}{2} \frac{n_c^2}{(n\tau)_{drag}} (T_e - T_c) + P_{c\text{-}i} = \frac{n_c^2}{(n\tau)_c} (\Phi_c + T_c)$$

Figure 12

ELECTRONS ARE CONFINED BY NET POSITIVE POTENTIAL

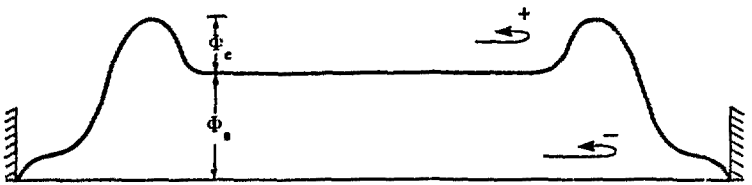

- Equality of loss rates fixes Φ_e/T_e

$$n\tau_{ee}\, g(R)\left(\frac{\Phi_e}{T_e}\right) \exp \frac{\Phi_e}{T_e} \approx (n\tau)_c$$

- Power balance determines T_e

$$2\frac{n_p^2 E_p}{(n\tau)_{drag}} V_p + P_{c-e} V_c$$

$$= \frac{3}{2}\frac{n_e^2 (T_e - T_c)}{(n\tau)_{drag}} V_c + (\Phi_e + T_e) j_c V_c + 2(\Phi_e + \Phi_c + T_e) j_p V_p$$

Figure 13

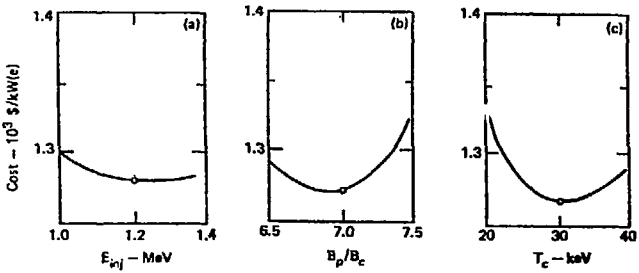

Figure 14: Effect on cost of 1000-MW(e) TMR's of variation in (a) injection energy E_{inj}, (b) vacuum mirror ratio between the center of the plug and the central cell B_p/B_c, and (c) temperature of the ions in the central cell T_c.

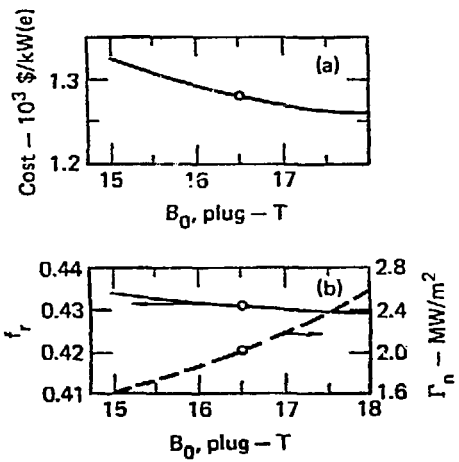

Figure 15: Effect on (a) predicted reactor cost and (b) recirculating power fraction f_r and neutron loading of the first wall Γ_n of variation in $B_{0,plug}$, the vacuum magnetic field strength at the center of the plug, for 1000-MW(e) TMR's with vacuum mirror ratio of the plug $R_{vac,plug} = 1.07$.

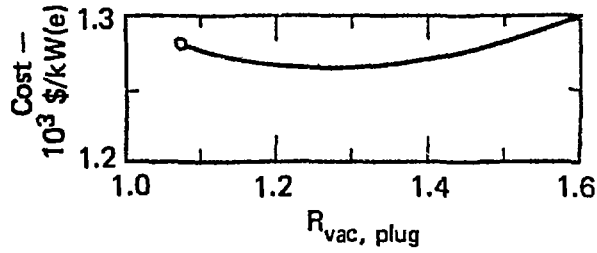

Figure 16: Predicted cost of optimized 1000-MW(e) THR's as a function of the vacuum mirror ratio of the plug $R_{vac,plug}$ for plug mirror field B_{mirror} = 17.7 T.

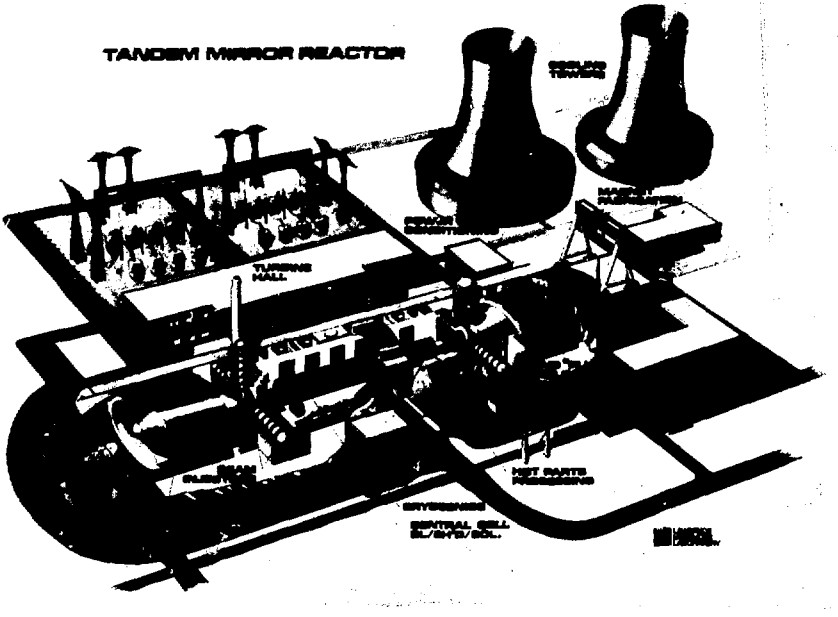

Figure 17

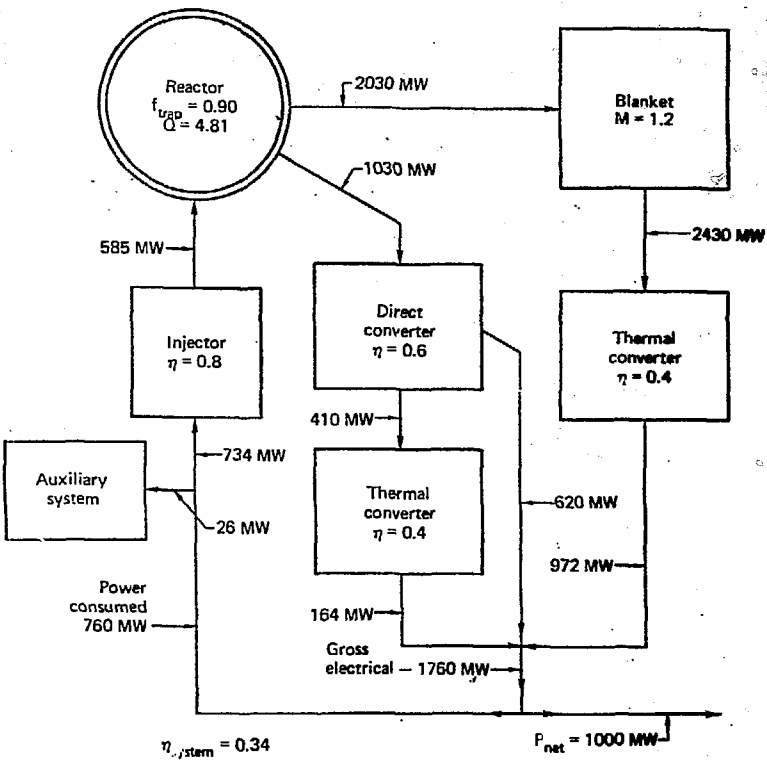

$$\text{Recirculating power fraction} = \frac{\text{power consumed}}{\text{gross electrical}} = 0.43$$

Figure 18: TMR power flow diagram.

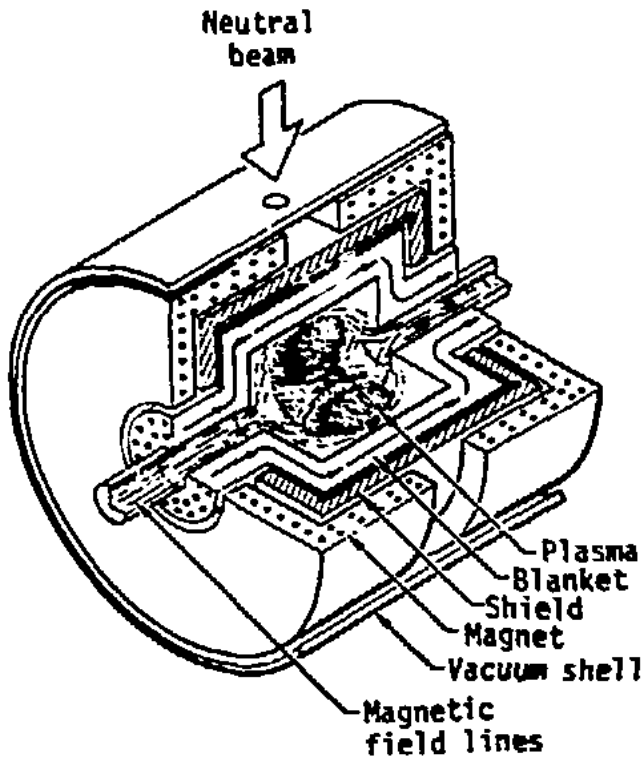

Figure 19: Schematic of Field-Reversed Mirror Reactor.

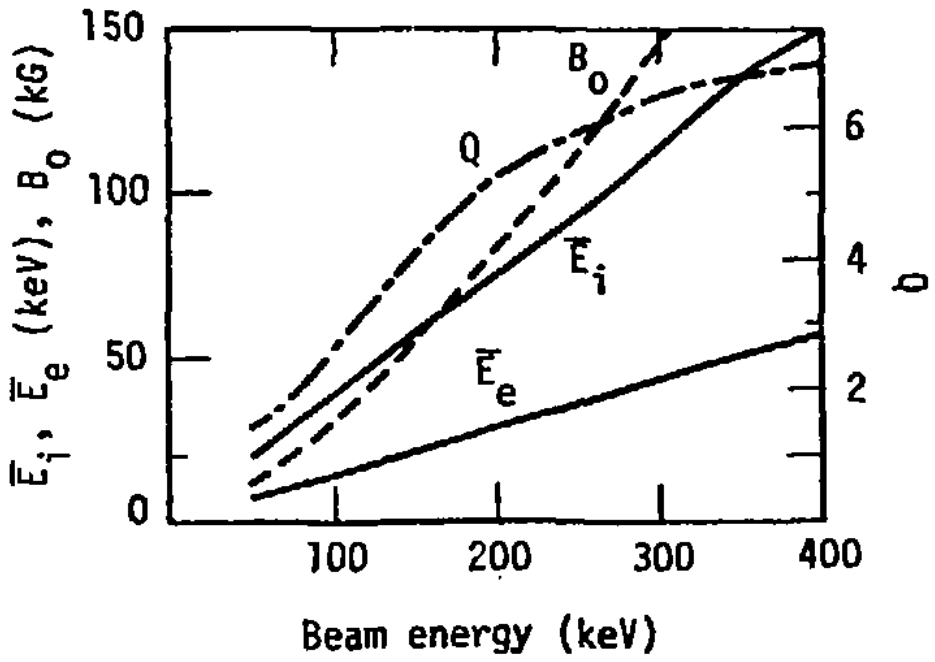

Figure 20: Mean ion and electron energies (E_i,E_e) magnetic field (B_0) and Q vs. neutral-beam energy for $a/\rho_i = 5$, $R_p/a = 2$, $L/R_p = 3$.

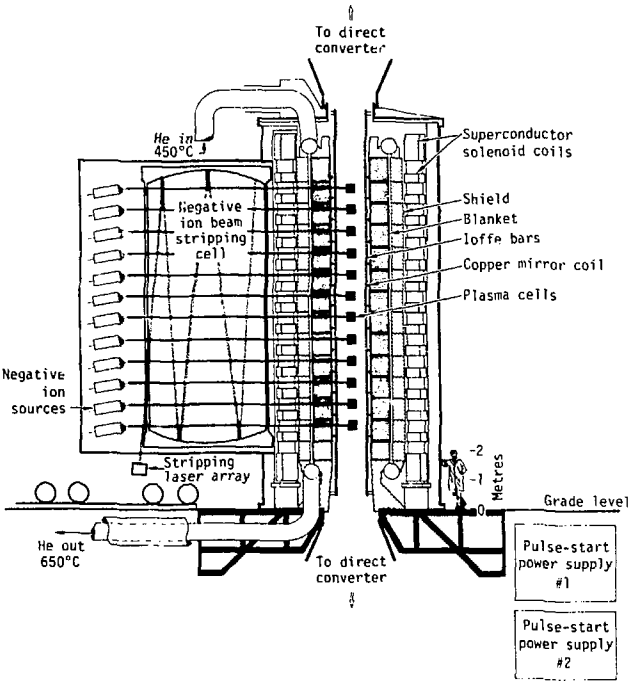

Figure 21: Layout of Multi-cell FRM Reactor.

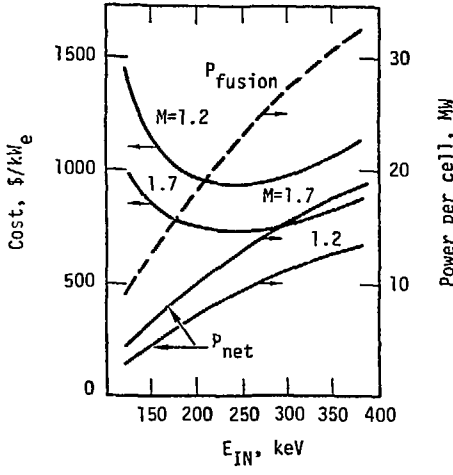

Figure 22: Power cost and fusion power vs. injection energy for optimum cell lengths.

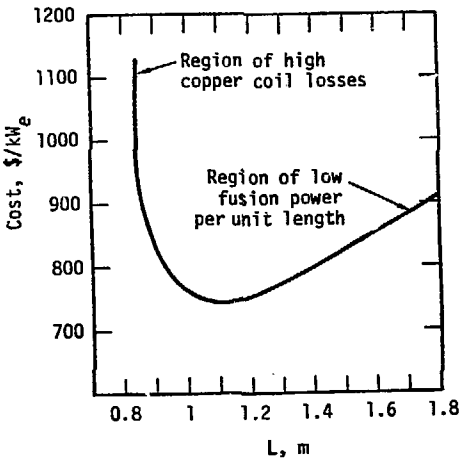

Figure 23: Projected cost of electrical power vs. cell length.